# Location of metallic elements in $(Co_{1-x}Fe_x)_2(OH)_2(C_8H_4O_4)$: use of MAD, neutron diffraction and $^{57}$Fe Mössbauer spectroscopy†

**Adel Mesbah, Bernard Malaman, Thomas Mazet, Romain Sibille and Michel François***

*Received 11th December 2009, Accepted 16th April 2010*
**DOI: 10.1039/b926144c**



Four samples of the solid solution $(Co_{1-x}Fe_x)_2(OH)_2(C_8H_4O_4)$ $x = 0.25$ (**1**), $x = 0.5$ (**2**), $x = 0.75$ (**3**); $x = 0.88$ (**4**) (*C*2/*m*) were investigated by synchrotron radiation using Multi-wavelength Anomalous Diffraction (MAD) and multipattern refinements in order to locate the two neighbour metallic elements Fe and Co. Although there is no cation ordering, the two metallic sites M1 (0, 0, 0) and M2 (0, 0.5, 0.5) are preferentially occupied by Co and Fe respectively. In this article we demonstrate that this distribution is in agreement with neutron data and $^{57}$Fe Mössbauer spectra at 100 K. Consequently, the MAD method can be used to locate close d-metallic elements in metal–organic frameworks.

## Introduction

Magnetic and structural properties of the metal–organic frameworks M(II)$_2$(OH)$_2$tp where M(II) is a divalent cation ($Fe^{2+}$, $Mn^{2+}$, $Co^{2+}$, $Cu^{2+}$) and tp is the terephthalate anion ($C_8H_4O_4^{2-}$) have been extensively studied by XRD and/or macroscopic magnetic measurements.[1,2,3,4] The $Co_2(OH)_2$tp compound is the only one of this series for which the magnetic structure has been determined by neutron diffraction.[4] This pure cobalt compound has an antiferromagnetic ground state ($T_N = 48$ K) but presents a complicated magnetic behavior as a function of the applied field.[1,4]

This article aims to describe the account of a study of the bimetallic system $(Co_{1-x}Fe_x)_2(OH)_2(C_8H_4O_4)$ based on the fact that Fe and Co compounds of this series are isotypes (SG = *C*2/*m*). The mixing of the two elements seems obvious and should be a way of tuning the magnetic properties. Limited research has been conducted on MOF bimetallic systems and it usually tends to purely deal with the macroscopic magnetic behavior.[5]

The structure of M(II)$_2$(OH)$_2$tp compounds exhibits two crystallographic independent sites M1 (0, 0, 0) and M2 (0, 0.5, 0.5). The main goal of this article is to determine the distribution of the metallic elements among these two sites in the hybrid solid solution $(Co_{1-x}Fe_x)_2(OH)_2(C_8H_4O_4)$. In order to demonstrate this three various techniques were used: (i) Multi-wavelength Anomalous Diffraction (MAD method) and the subsequent multipattern Rietveld refinements. Due to the small difference in X-ray form factors between Fe and Co, X-ray powder diffraction experiments were realized on a synchrotron line using different source energies (near the K threshold of Fe and Co) in order to magnify their differentiation. A similar procedure was already been successfully applied to a large number of crystalline materials, some examples are given in ref. 6. (ii) Neutron diffraction, because the scattering lengths values of Fe and Co are different enough to distinguish these two elements. (iii) $^{57}$Fe Mössbauer spectroscopy.

## Experimental

### Synthesis and chemical analysis

**Synthesis.** The compounds of the solid solution $(Co_{1-x}Fe_x)_2(OH)_2$(tp) were synthesized by a hydrothermal route from a mixture of $CoCl_2 \cdot 6H_2O$ (Aldrich, 98%), $FeCl_2 \cdot 4H_2O$ (Aldrich, 98%) and disodium terephthalate $Na_2C_8H_4O_4$ (Aldrich, 98%) dissolved in 10 ml of distilled water. Five samples corresponding to various $x$ values were synthesized. **1**, $x = 0.25$, $CoCl_2 \cdot 6H_2O$ (1.94 g, 8.15 mmol); $FeCl_2 \cdot 4H_2O$ (0.555 g, 2.81 mmol), $Na_2C_8H_4O_4$ (4.63 g, 22.04 mmol), **2**, $x = 0.50$, $CoCl_2 \cdot 6H_2O$ (0.688 g, 2.89 mmol); $FeCl_2 \cdot 4H_2O$ (0.576 g, 2.89 mmol), $Na_2C_8H_4O_4$ (2.34 g, 11.1 mmol), **3**, $x = 0.75$, $CoCl_2 \cdot 6H_2O$ (0.86 g, 3.61 mmol); $FeCl_2 \cdot 4H_2O$ (1.74 g, 8.75 mmol), $Na_2C_8H_4O_4$ (4.58 g, 21.8 mmol), **4**, $x = 0.88$, $CoCl_2 \cdot 6H_2O$ (0.194 g, 0.81 mmol); $FeCl_2 \cdot 4H_2O$ (1.18 g, 5.94 mmol), $Na_2C_8H_4O_4$ (2.12 g, 10.1 mmol), **5**, $x = 1.0$, $FeCl_2 \cdot 4H_2O$ (1.43 g, 7.19 mmol), $Na_2C_8H_4O_4$ (2.27 g, 10.79 mmol). The pH of the solutions was kept at 8 by adding an aqueous solution of NaOH. The initial mixture (~20 ml) was kept under magnetic stirring for 5 min then transferred into a 25 ml Teflon-walled acid digestion bomb, and subsequently heated under autogenous pressure for 72 h at 150 °C. The reaction product was collected by filtration, washed twice with a mixture of distilled water–anhydrous ethanol (1 : 1) and then dried at room temperature.

**Chemical analysis.** Metallic compositions of samples **1** to **4** were measured by Electron Probe Micro Analysis (EPMA). They correspond well to the nominal compositions given in Table 1. EPMA results are reported in the ESI (Table S1†).

### Synchrotron measurements

Powder X-ray diffraction experiments were carried out at Swiss Light Source using the MS-powder beam line.[7] Diffraction patterns of the powder samples were measured in glass capillaries ($\phi = 0.3$ mm) with the standard Debye-Scherrer geometry using

*Institut Jean Lamour – UMR 7198, Nancy Université – 54506 Vandoeuvre les Nancy, France. E-mail: Michel.Francois@lcsm.uhp-nancy.fr; Fax: +33-3-83684611; Tel: +33-3-83684658*

† Electronic supplementary information (ESI) available: Electron Probe Micro Analysis of compounds **1** to **5**, refined atomic coordinates from synchrotron and neutron experiments and selected interatomic distances. See DOI: 10.1039/b926144c

 

**Table 1** Synchrotron crystallographic data and Rietveld refinement parameters for each set of three patterns (see text): I (Fe K edge), II (Co K edge) and III (higher energy)

| Compound | **1** | **2** | **3** | **4** |
|---|---|---|---|---|
| Structural formula | $(Co_{0.75}Fe_{0.25})_2(OH)_2(C_8H_4O_4)$ | $(Co_{0.50}Fe_{0.50})_2(OH)_2(C_8H_4O_4)$ | $(Co_{0.25}Fe_{0.75})_2(OH)_2(C_8H_4O_4)$ | $(Co_{0.12}Fe_{0.88})_2(OH)_2(C_8H_4O_4)$ |
| Formula weight (g mol$^{-1}$) | 314.45 | 312.91 | 311.37 | 310.57 |
| $T$ (K) | 100 | 100 | 100 | 100 |
| System | Monoclinic | Monoclinic | Monoclinic | Monoclinic |
| Space group | *C*2/*m* | *C*2/*m* | *C*2/*m* | *C*2/*m* |
| $a$ (Å) | 19.9218(3) | 19.9172(3) | 19.9104(3) | 19.8980(3) |
| $b$ (Å) | 3.2882(1) | 3.3084(1) | 3.3253(1) | 3.3409(1) |
| $c$ (Å) | 6.2923(1) | 6.2974(1) | 6.3052(1) | 6.3116(1) |
| $\beta$ (°) | 95.67(1) | 95.56(1) | 95.37(1) | 95.15(1) |
| $V$ (Å$^3$) | 410.17(2) | 413.00(1) | 415.61(1) | 417.89(1) |
| $Z$ | 2 | 2 | 2 | 2 |
| Dx (g cm$^{-3}$) | 2.55 | 2.52 | 2.49 | 2.47 |
| Abs. Coef. [$\mu_{xr}$] [I;II;III] | 0.35; 0.63; 0.26 | 0.34; 0.98; 0.25 | 0.33; 1.33; 0.25 | 0.33; 1.51; 0.24 |
| Angular range 2$\theta$ (°) [I;II;III] | 8–117; 7.5–117; 4-75 | 8–117; 8–78; 4-79 | 9–117, 7–80, 4-80 | 7.5–117; 8–68; 4–94 |
| Nobs [I;II;III] | 14 568; 14 634; 9457 | 14 568; 9326; 10 038 | 14 260; 9725; 10 011 | 14 396; 7770; 11 774 |
| Nref [I;II;III] | 243; 313; 2312 | 244; 133; 1010 | 247; 140; 1028 | 247; 97; 1501 |
| $R_p$ (%) [I;II;III] | 5.02; 1.62; 6.00 | 3.77; 1.31; 6.86 | 3.88; 1.10; 5.96 | 4.04; 1.07; 7.73 |
| $R_{wp}$ (%) [I;II;III] | 6.89; 2.31; 6.12 | 6.26; 1.99; 6.05 | 5.54; 1.60; 5.49 | 5.43; 1.43; 6.17 |
| $R_{Bragg}$ (%) [I;II;III] | 9.99; 13.8; 8.42 | 11.9; 21.1; 13.0 | 9.71; 14.3; 9.82 | 11.0; 22,1; 10.7 |
| $R_F$ (%) [I;II;III] | 9.40; 10.9; 5.75 | 7.38; 14.0; 8.90 | 7.67; 9.50; 8.14 | 8.90; 16.3; 8.99 |
| No. of profile parameters[I;II;III] | 12; 12; 12 | 12; 12; 12 | 12; 12; 12 | 12; 12, 12 |
| No. of intensity dependent parameters | 25 | 25 | 25 | 25 |
| No. of soft constraints[a] | 6 | 6 | 6 | 6 |

[a] C1–O1 = 1.270(5) Å; C1–O2 = 1.270(5) Å; C1–C2 = 1.54(1) Å; C2–C4 = 1.40(1) Å; C2–C3 = 1.40(1) Å; C3–C4 = 1.400(5) Å. Compositions of **0** (see ref. 1) and **5** (see ref. 2) are $Co_2(OH)_2(C_8H_4O_4)$ and $Fe_2(OH)_2(C_8H_4O_4)$ respectively. Atomic coordinates are given in Table S2, ESI.

a multistrip detector.[8] Three powder diffraction patterns were recorded for each sample, two of the patterns using X-ray energies near the K edge of each metallic element ($\lambda_{Fe}$ = 1.7499 and $\lambda_{Co}$ = 1.6135 Å), *i.e.* where scattering factors vary by resonant effects, and a third at a higher energy ($\lambda_{HighEn}$ = 0.7999 Å), *i.e.* far from the edges. The one-dimensional detector allowed us to measure entire diffraction patterns over 120° in a few seconds, depending on the crystallinity of the sample. For each study, four diffraction patterns corresponding to four different positions of the detector were measured in order to improve Bragg intensity to background ratios. Those diffraction patterns were measured *via* the local software piloting the diffractometer and averaging the data recorded at around 10 s per position. Furthermore, the diagrams were recorded at 100 K using a cryo jet device in order to decrease the Debye–Waller factor and therefore increase the resolution. A typical pattern is shown in Fig. 1. The energies were calibrated using silicon from NIST. The dispersion coefficients used in the Fullprof software are reported in Table 2. They were determined by using the DISPANO V.2 program[9] and the Brennan and Cowan data.[10]

**Le Bail decomposition.** The two-theta ranges used are reported in Table 1. The line profiles were modeled using function 7 of the Fullprof_Suite[11] (Thompson–Cox–Hastings pseudo-Voigt convoluted with axial divergence asymmetry function). The instrumental function was measured by using a small line-width sample (NAC; $Na_2Ca_3Al_2F_4$) as a reference. The line broadening was interpreted by microstructural effects (size and microstrain) as it is implemented in Fullprof_Suite for the Le Bail decomposition. A total of 12 parameters were refined for each pattern: 4 for the crystallite size, 3 for the strain, 4 for the lattice, 1 for the

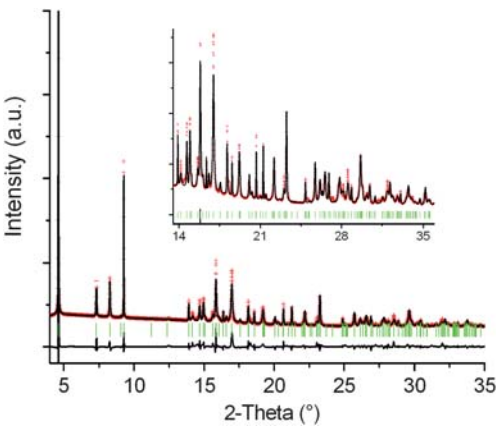


**Fig. 1** Rietveld diagram of **4** ($\lambda$ = 0.799876 Å) showing observed (red), calculated (black) and difference patterns. Bragg positions are represented by green lines.

**Table 2** Energies and dispersion coefficients used for the three-pattern refinements

| Edge | $E$ (eV) | $\lambda^a$ (Å) | $f'$ | $f''$ | M |
|---|---|---|---|---|---|
| $K_{Fe}$ | 7085.2 | 1.749882 | −5.321 | 0.473 | Fe |
| | | | −2.178 | 0.557 | Co |
| $K_{Co}$ | 7684.0 | 1.613470 | −5.458 | 0.477 | Co |
| | | | −1.792 | 3.355 | Fe |
| HighEn. | 15500.6 | 0.799876 | 0.356 | 1.038 | Fe |
| | | | 0.344 | 1.191 | Co |

[a] Refined with Si standard.

zero position. $R_p$ and $R_{wp}$ factors converge satisfactorily to values lower than 5%.

**Multipattern Rietveld refinement.** The starting structural model was taken from ref. 1. 25 additional intensity dependant parameters were refined including 3 scale factors, 17 atomic coordinates, 4 isotropic thermal factors (1 for each O and C species, 1 for each metallic site) and 1 parameter for the occupancy factors of the two sites M1 and M2, constraining the global metallic compositions to have the EPMA value. Absorption effects due to the thickness of the samples had the same influence on the refined scale and occupancy factors. To avoid systematic errors on the distribution of the elements, an absorption correction coefficient, varying for each sample, was applied to correct the intensities. Values of $[\mu_{xr}]$ used for the refinements take into consideration that the powder density in the capillaries is a third of the theoretical one. In most of the cases, the $[\mu_{xr}]$ coefficients were lower than one (see Table 1). Nevertheless corrections were applied in order to increase the accuracy.

### Neutron measurements

Powder neutron diffraction experiments were carried out at the Institut Laue Langevin (ILL), Grenoble (France) using the D1b two-axis diffractometer ($\lambda$ = 2.52 Å, step of 0.2°). Diffraction patterns of samples **1**, **2** and **4** were recorded at 100 K using a standard helium cryostat. The analysis of the data was performed by Rietveld profile refinements using the Fullprof software.[11] Crystallographic data and refinements parameters are reported in Table 3. The Rietveld diagram for **2** is shown in Fig. 2. According to the well contrasted neutron scattering lengths of Fe and Co atoms (scattering lengths: $b_{Fe}$ = $0.96.10^{-12}$ cm and $b_{Co} = 0.25.10^{-12}$ cm), the occupancy factors of the two metallic sites M1 and M2 (namely the ratio of Fe to Co on each site) have been refined constraining the global metallic compositions to have the EPMA values.

### $^{57}$Fe Mössbauer spectroscopy

$^{57}$Fe Mössbauer spectra were recorded at 100 K (in an Air Liquide cryostat) using a constant acceleration spectrometer with 1024 channels. The source was 20 mCi $^{57}$Co in a rhodium matrix. The data were analyzed with a least-squares fitting program assuming Lotentzian peaks.[12] The program gives the quadrupole splitting $\Delta$ and the isomer shift $\delta$ with respect to α-iron at room temperature.

**Table 3** Neutron crystallographic data and Rietveld refinement parameters (atomic coordinates are given in Table S2, ESI)

| Compound | **1** | **2** | **4** |
|---|---|---|---|
| $a$ (Å) | 19.92(1) | 19.92(1) | 19.90(1) |
| $b$ (Å) | 3.29(1) | 3.31(1) | 3.34(1) |
| $c$ (Å) | 6.29(1) | 6.30(1) | 6.31(1) |
| $\beta$ (°) | 95.7 | 95.6 | 95.2 |
| $2\theta$ (°) range | 3.0–83.8 | 3.0–83.8 | 3.0–83.8 |
| Nobs of points | 400 | 400 | 400 |
| No. of ind. refl. | 114 | 115 | 114 |
| $R_p$ (%) | 1.0 | 1.0 | 1.0 |
| $R_{wp}$ (%) | 1.25 | 1.4 | 1.4 |
| $R_{Bragg}$ (%) | 10.2 | 10.0 | 5.0 |
| $R_F$ (%) | 9.7 | 9.4 | 4.3 |
| No. of profile parameters | 11 | 11 | 11 |
| No. of intensity parameters | 29 | 29 | 29 |
| No. of soft constraints[a] | 9 | 9 | 9 |

[a] The same as for X-ray plus OH–H1 = C4–H4 = C3–H2 = 0.98(1).

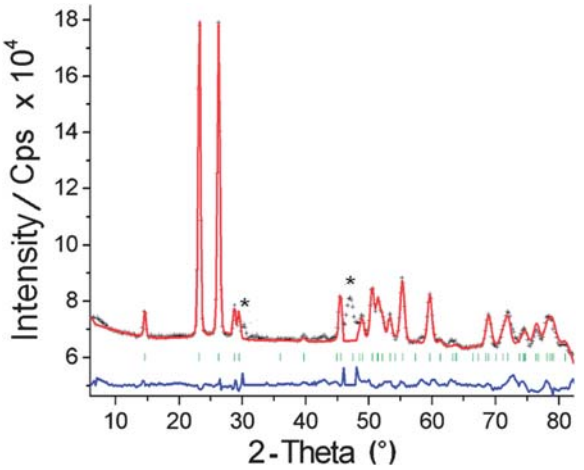


**Fig. 2** Neutron Rietveld diagram of **2** (data taken at 100 K). Stars above some reflections correspond to terephthalate impurities visible due to the very negative neutron scattering length of hydrogen atoms.

## Results and discussion

A typical Rietveld diagram from X-ray synchrotron data is shown in Fig. 1. The anomalous effect on the relative intensities is illustrated in Fig. 3, showing a selected $2\theta$ range of the X-ray powder diffraction patterns for the three wavelengths.

### Lattice parameters

The lattice refinement (profile matching by Le Bail decomposition) confirms the existence of a solid solution and not a combination of two phases. The variation of the lattice volume as a function of the iron concentration is shown in Fig. 4. The volume increases with the Fe-content, following a Vegard's law, which is in agreement with the ionic radii given by the Shannon's tables[13] ($r$Fe$^{2+}$ = 0.780 Å, $r$Co$^{2+}$ = 0.745 Å for octahedrally O-coordinated cations in a high spin configuration).

### Interatomic distances

The structure of the $Fe_2(OH)_2(C_8H_4O_4)$ compound is shown in Fig. 5. It is characterized by the occurrence of two independent M1 (0, 0, 0) and M2 (0, 0.5, 0.5) sites among which the Fe and Co atoms are distributed in the $(Co_{1-x}Fe_x)_2(OH)_2(C_8H_4O_4)$ solid solutions. Although they both have an octahedral coordination polyhedron, the environments of M1 and M2 are quite different. M1 site is at the center of an octahedron formed by four hydroxide ions and two O-carboxylate atoms whereas the M2 octahedron is formed by four O-carboxylate atoms and two hydroxide ions. The $M_i$–O distances, obtained from the resonant diffraction method (*high resolution data*) for all members of $(Co_{1-x}Fe_x)_2(OH)_2(C_8H_4O_4)$ solid solution, are reported in the ESI (Table S3†). When $x$ increases from 0.25 to 0.88, the average

 

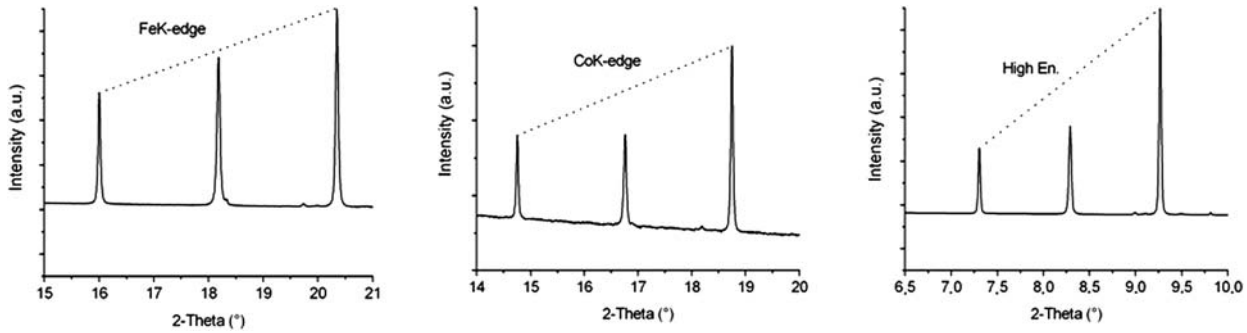


**Fig. 3** Selected part of the XRPD pattern of **4** showing the anomalous effect on the relative intensities.

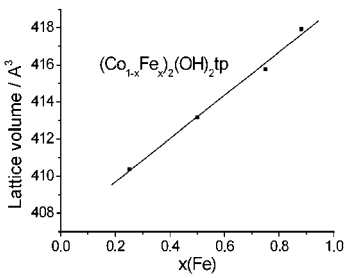


**Fig. 4** Lattice volume *vs.* Fe content from synchrotron data at 100 K.

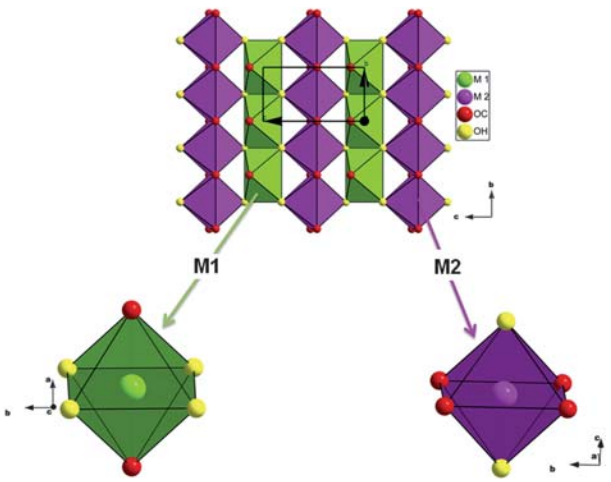


**Fig. 5** Structure of metal–hydroxide layers and polyhedral representation of the M1 and M2 site environments.

distances M1–O and M2–O increase from 2.127 to 2.149 Å (1.03% elongation) and from 2.133 to 2.163 Å (1.4% elongation) respectively. It is in agreement with the preferential occupancy of the M2 site by the larger $Fe^{2+}$ ions.

### Distribution of Fe and Co atoms

The distribution of Fe and Co atoms in the M1 and M2 sites *vs.* iron-content, deduced from resonant diffraction experiments (squares) and neutron diffraction data (triangles), is reported in Fig. 6. Both techniques clearly show that Fe and Co atoms occupy both of the two available sites. However, they support

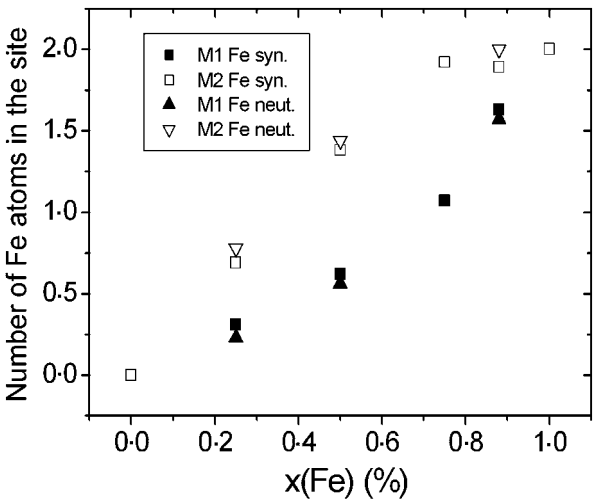


**Fig. 6** Distribution of Fe *vs.* Fe-content.

a marked preference of $Fe^{2+}$ ions for the M2 site. This result is used during the analysis of the $^{57}Fe$ Mössbauer spectra (see below). Neutron and synchrotron data agree comparatively well, thus validating the MAD method for our compounds.

Furthermore, it is significant to note that due to the important non coherent scattering of H-atoms and the subsequent decrease of the signal-to-noise ratio, the neutron diffraction technique implies the use of deuterated samples for rich H-atom compounds. In this study, samples were not deuterated but it can be expected that in the case of MOFs with larger H-atom contents than terephthalate based compounds ($w_{at}H = 27\%$ in **1–5**), MAD can thus be used favorably.

### Mössbauer spectra at 100 K

According to the occurrence of two independent cation sites in the structure of the $(Co_{1-x}Fe_x)_2(OH)_2(C_8H_4O_4)$ compounds, data have been analyzed with two quadrupolar doublets. Labelling the four absorption peaks from **a** to **d**, as shown in spectrum 5 of Fig. 7 (*i.e.* $Fe_2(OH)_2(C_8H_4O_4)$), two sets of hyperfine parameters could be deduced:

D1 (between **b** and **c**) with IS = 1.24 mm $s^{-1}$, EQ = 2.14 mm $s^{-1}$; D2 (between **a** and **d**) with IS = 1.29 mm $s^{-1}$, EQ = 2.80 mm $s^{-1}$.

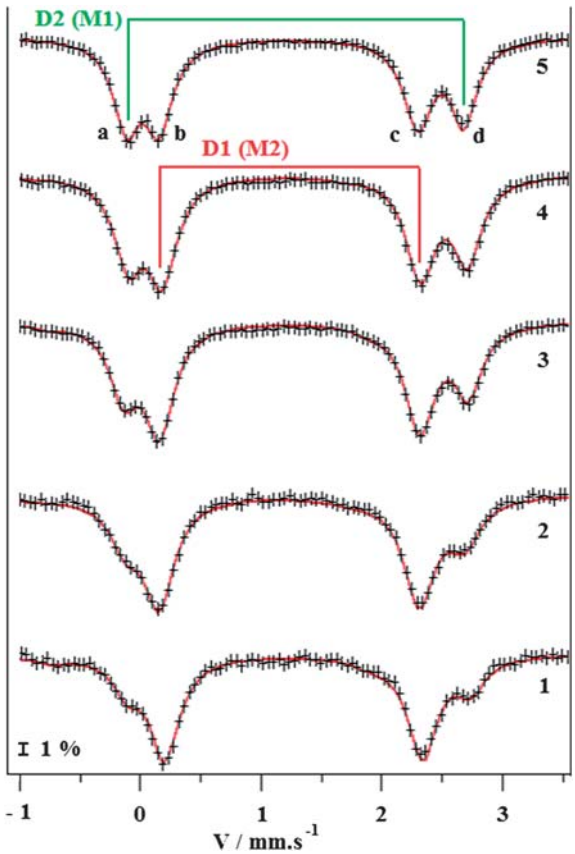


**Fig. 7** Mössbauer spectra for the 1 to 5 terms of the $(Co_{1-x}Fe_x)_2(OH)_2(C_8H_4O_4)$ solid solution (namely, $x = 0.25$, 0.50, 0.75, 0.88 and 1, respectively).

D′1 (between **a** and **c**) with IS = 1.12 mm $s^{-1}$, EQ = 2.40 mm $s^{-1}$; D′2 (between **b** and **d**) with IS = 1.35 mm $s^{-1}$, EQ = 2.50 mm $s^{-1}$.

The study of the whole solid solution allowed us to explore this point. Fig. 7 shows Mössbauer spectra of samples **1** to **5**. The presence of two doublets for all members of the solid solution confirms the absence of a total ordering in the distribution of Fe and Co onto the two M1 and M2 sites.

One observes a large decrease of the intensity of the **a** and **d** peaks with $x$ decreasing. This result unambiguously leads us to choose the D1/D2 hypothesis (see Fig. 7) and, according to the conclusions of the diffraction studies, to attribute D2 to the M1 site and D1 to the M2 site.

The refined hyperfine parameters are reflected in Table 4. It is worth noting that in all cases, the isomer shift is characteristic of a $Fe^{2+}$ ion. The area values of each quadrupolar doublet ($I_{Möss}$ %) and the corresponding calculated values as deduced from the diffraction studies ($I_{Diff}$) are also reported in this table. Their comparison shows that the Mössbauer data clearly confirm the conclusions of the diffraction experiments.

**Table 4** Hyperfine parameters $\Gamma$, $\delta$ and $\Delta$ ($\pm$ 0.05 mm $s^{-1}$) for the solid solution $Co_{2-x}Fe_x(OH)_2tp$ at 100 K

| Compound | Signal | $I_{Moss}$ (%) | Site | $I_{Diff}$ (%) | $\Gamma$ | $\delta$ | $\Delta$ |
|---|---|---|---|---|---|---|---|
| **5** | $D_1$ | 52 | M2 | 50 | 0.28 | 1.24 | 2.14 |
| | $D_2$ | 48 | M1 | 50 | 0.28 | 1.29 | 2.80 |
| **4** | $D_1$ | 54 | M2 | 54 | 0.28 | 1.24 | 2.14 |
| | $D_2$ | 46 | M1 | 46 | 0.28 | 1.29 | 2.80 |
| **3** | $D_1$ | 62 | M2 | 64 | 0.29 | 1.24 | 2.16 |
| | $D_2$ | 38 | M1 | 36 | 0.27 | 1.29 | 2.85 |
| **2** | $D_1$ | 70 | M2 | 69 | 0.31 | 1.23 | 2.16 |
| | $D_2$ | 30 | M1 | 31 | 0.31 | 1.28 | 2.81 |
| **1** | $D_1$ | 78 | M2 | 78 | 0.30 | 1.27 | 2.13 |
| | $D_2$ | 22 | M1 | 22 | 0.27 | 1.31 | 2.84 |

## Conclusions

The study of the solid solution $(Co_{1-x}Fe_x)_2(OH)_2(C_8H_4O_4)$ ($C2/m$) with $0.25 \leq x < 1$ by synchrotron radiation (resonant diffraction), neutron diffraction and $^{57}Fe$ Mössbauer spectroscopy has allowed the location of iron and cobalt ions in the two independent sites of the structure. Although there is no cation ordering, the two metallic sites M1 (0, 0, 0) and M2 (0, 0.5, 0.5) are preferentially occupied by Co and Fe ions, respectively.

The MAD method provides consistent results with neutron diffraction and $^{57}Fe$ Mössbauer spectroscopy. As the neutron diffraction can not be used when the H content of the samples is too high (otherwise, deuterated samples are needed) the MAD method can be employed favorably for MOFs containing more extended organic moieties and consequently high H content.

Magnetic properties of samples **1–5**, and similar solid solutions containing other d-element couples (Fe–Mn, Co–Mn…) are under study.

## Acknowledgements

The authors are grateful to Fabia GOZZO from Swiss Light Source for his help in the diffraction experiments with the synchrotron radiation. We are indebted to the Institut Laue Langevin (Grenoble, France) for the provision of research facilities. Our local contact (S. Capelli) is warmly acknowledged for her assistance during the recording of the neutron patterns.

## Notes and references

1 Z. L. Huang, M. Drillon, N. Masciocchi, A. Sironi, J. T. Zhao, P. Rabu and P. Panissod, *Chem. Mater.*, 2000, **12**, 2805.
2 A. Carton, A. Mesbah, M. François and P. Rabu, *Z. Kristallogr., Suppl.*, 2007, **26**, 581–586.
3 P. Rabu, Z. L. Huang, C. Hornick and M. Drillon, *Synth. Met.*, 2001, **122**, 509–515; P. Rabu, J. M. Rueff, Z. L. Huang, S. Angelov, J. Souletie and M. Drillon, *Polyhedron*, 2001, **20**, 1677–1685; S. Abdelouhab, M. François, E. Elkaim and P. Rabu, *Solid State Sci.*, 2005, **7**, 227.
4 R. Feyerherm, A. Loose, P. Rabu and M. Drillon, *Solid State Sci.*, 2003, **5**, 321–326.
5 Y. J. Kim, D. Y. Jung, K. P. Hong and G. Demazeau, *Solid State Sci.*, 2001, **3**, 837–846; M. H. Zeng, B. Wang, X. Y. Wang, W. X. Zhang, X. M. Chen and S. Gao, *Inorg. Chem.*, 2006, **45**, 7069–7076; S. Fernandez, J. L. Mesa, J. L. Pizarro, A. Pena, J. Gutiérrez, M. I. Arriortua and T. Rojo, *J. Magn. Magn. Mater.*, 2004, **272–276**, 1113–1115; M. Taibi, S. Ammar, N. Jouini and F. Fiévet, *J. Phys. Chem. Solids*, 2006, **67**, 932–937; I. Gil de Muro, L. Lezama, M. Insausti and T. Rojo, *Polyhedron*, 2004, **23**, 929–936.
6 P. Lee, Y. Gao, H. S. Sheu, V. Petricek, R. Restori, P. Coppens, A. Darovskikh, J. C. Phillips, A. W. Sleight and M. A. Subramanian, *Science*, 1989, **244**, 62–63; A. P. Wilkinson, A. K. Cheetham, S. C. Tang and W. J. Reppart, *J. Chem. Soc., Chem. Commun.*, 1992, 1485–1487; M. Helliwell, *J. Synchrotron Radiat.*, 2000, **7**, 139–147; J. M. Joubert, R. Cerny, M. Latroche,

 

A. Percheron-Guégan and K. Yvon, *J. Appl. Crystallogr.*, 1998, **31**, 327–332; A. R. Cowley, R. H. Jones, S. J. Teat and A. M. Chippindale, *Microporous Mesoporous Mater.*, 2002, **51**, 51–64; J. M. Joubert, R. Cerny and H. Emerich, *Z. Kristallogr., Suppl.*, 2007, **26**, 311–316; F. Zamoum, M. François, J. Tobola, E. Elkaim and M. Vilasi, *Intermetallics*, 2008, **16**, 1237–1244.

7 B. D. Patterson, R. Abela, H. Auderset, Q. Chen, F. Fauth, F. Gozzo, G. Ingold, H. Kühne, M. Lange, D. Maden, D. Meister, P. Pattison, Th. Schmidt, B. Schmitt, C. Schulze-Briese, M. Shi, M. Stampanoni and P. R. Willmott, *Nucl. Instrum. Methods Phys. Res., Sect. A*, 2005, **540**, 42–67.

8 A. Bergamaschi, C. Broennimann, R. Dinapoli, E. Eikenberry, F. Gozzo, B. Henrich, M. Kobas, P. Kraft, B. Patterson and B. Schmitt, *Nucl. Instrum. Methods Phys. Res., Sect. A*, 2008, **591**, 163–166.

9 LMGP-Suite Suite of Programs for the interpretation of X-ray Experiments, by Jean laugier and Bernard Bochu, ENSP/ Laboratoire des Matériaux et du Génie Physique, BP 46. 38042 Saint Martin d'Hères, France. http://www.inpg.fr/LMGP and http://www.ccp14.ac.uk/tutorial/lmgp/.

10 S. Brennan and P. L. Cowan, *Rev. Sci. Instrum.*, 1992, **63**, 850.

11 J. Rodriguez-Carvajal, M. T. Fernandez-Diaz and J. L. Martinez, *J. Phys.: Condens. Matter*, 1991, **3**, 3215.

12 G. Lecaer, private communication.

13 R. D. Shannon, *Acta Crystallogr., Sect. A: Cryst. Phys., Diffr., Theor. Gen. Crystallogr.*, 1976, **32**, 751–767.